Nat Hazards (2015) 78:995–1020
DOI 10.1007/s11069-015-1754-2

ORIGINAL PAPER

Simulation of the records of the 27 March 2013 Nantou Taiwan earthquake using modified semi-empirical approach

A. Joshi[1] · Chun-Hsiang Kuo[2] · Piu Dhibar[1] · Sandeep[1] · M. L. Sharma[3] · Kuo-Liang Wen[4] · Che-Min Lin[2]

Received: 14 August 2014 / Accepted: 8 April 2015 / Published online: 3 May 2015

Abstract It is seen that strong motion generation area plays an important role in the shaping of strong motion records at the observation point. Strong motion generation areas identified within the rupture plane of the 27 March 2013 Nantou, Taiwan, earthquake ($M_w = 5.9$) have been modelled in this work. It is seen that all available records are at the surface which include site amplification terms. The modified semi-empirical technique effectively simulates records at rock site. The site amplification terms in all records have been removed using SHAKE 91 program and velocity input at each site. The observed records corrected for site amplification terms are further used for comparison with simulated record at the bedrock from several models. Once the observed records at soil sites are transferred at the bedrock, the next task is selection of final model that gives best fit records. Peak ground acceleration from simulated record at four sites is compared with that from corrected observed data. Since the semi-empirical technique of simulation is strongly dependent on various modelling parameters such as dip, strike, rake, rupture velocity and starting points of rupture, these parameters change iteratively in a specified range in a heuristic way to obtain best modelling parameters. The model giving minimum root mean square error (RMSE) is retained at final model. It is seen that minimum root mean square error of the wave form comparison has been obtained at four stations for the source model having single strong motion generation area. Strong motion records have been simulated at four different recording stations. Comparison of observed and simulated records has been made in terms of RMSE between simulated and observed acceleration records, velocity records and the response spectra at each of four stations. Comparison of waveforms and parameters extracted from observed and simulated records confirms the efficacy of the modified technique to model earthquake characterized by SMGAs.

✉ Piu Dhibar
piu.dhibar89@gmail.com

[1] Department of Earth Sciences, Indian Institute Technology Roorkee, Roorkee, India

[2] National Center for Research on Earthquake Engineering, Taipei, Taiwan

[3] Department of Earthquake Engineering, Indian Institute of Technology Roorkee, Roorkee, India

[4] Department of Earth Sciences, National Central University, Taoyuan, Taiwan

Keywords Strong ground motion · Semi-empirical · Nantou earthquake · Strong motion generation areas

1 Introduction

Any seismically active region needs reliable predictions of strong motion parameters for designing of the earthquake-resistant structures. These parameters can be predicted through simulation of the strong motion data for a given site. Such prediction is possible only with the help of different simulation methods. Methods of simulation of strong ground motion can be classified into three broad categories. First method is composite source modelling technique given by Zeng et al. (1994), Yu (1994), Yu et al. (1995), Saikia and Herrmann (1985) and Saikia (1993). Second method of simulation is stochastic simulation of high-frequency strong ground motion which is given by Housner and Jennings (1964), Hanks and McGuire (1981), Boore (1983), Boore and Atkinson (1987) and Lai (1982). Third method is empirical green's function (EGF) method given by Hartzell (1978, 1982), Kanamori (1979), Hadley and Helmberger (1980), Mikumo et al. (1981), Irikura and Muramatu (1982), Irikura (1983,1986), Irikura and Kamae (1994), Munguia and Brune (1984) and Hutchings (1985). Among all of the above methods of simulation empirical green's function (EGF) technique is most reliable simulation method for simulation of strong ground motion data. This method was initially introduced by Hartzell (1978), and modification in this technique has been made by Kanamori (1979), Irikura (1983), Munguia and Brune (1984) and Irikura (1986). In empirical green's function (EGF) technique, the major limitation is the requirement of aftershock event at every respective site of simulation. In the recent years, the semi-empirical technique has evolved as an effective tool for strong ground motion simulation. This method has been initiated by Midorikawa (1993) for modelling of the rupture buried in a homogeneous earth model modification that has been made by Joshi et al. (2001), Joshi and Midorikawa (2004) and Joshi et al. (2012a) to consider the effect of layered model in the technique. This method has advantage of both empirical green's function (EGF) technique and Stochastic simulation technique and has been applied to investigate many strong motion earthquakes (Joshi and Patel 1997; Joshi et al. 1999; Kumar and Khattri 1999; Joshi 2001; Joshi et al. 2001; Joshi 2004; Joshi and Midorikawa 2004; Joshi and Mohan 2008; Joshi et al. 2012a, b, 2014). One of the major constraints in this method is the requirement of attenuation relation applicable for the place of simulation. Joshi et al. (2012a) have removed dependency of this method on attenuation relation of that area by theoretical relation based on seismic moment, radiation pattern and shear wave velocity and hypocentral distance. Joshi et al. (2012b) have further modified this technique for component-wise simulation of the strong motion records. It has been demonstrated by Miyake et al. (2003) that high-frequency strong motion due to earthquake is modelled successfully by strong motion generation area, which is identified as an area characterized by large uniform slip velocity within the total rupture area. Miyake et al. (2003) have modelled Kagoshima earthquake ($M_w = 6.1$) of 1997, Yamaguchi earthquake ($M_w = 5.9$) of 1997 and Iwate earthquake ($M_w = 6.1$) of 1998 by incorporating strong motion generation area using empirical green's function technique. Empirical green's function technique has been successfully used by Kamae and Kawabe (2004), Miyahara and Sasatani (2004), Suzuki and Iwata (2007) and Takiguchi et al. (2011) to model the effect of strong motion generation area in the source model of earthquake. Though the use of empirical green's function is effective for strong motion generation area, it still suffers from major

constraints of requirement of adequate aftershock at the point of simulation. It is noticed that the replacement of aftershock by the envelope of accelerogram used in the semi-empirical technique gives a reliable comparison between simulated and the observed strong motion records. Recently, Joshi et al. (2014) modified technique to incorporate the effect of SMGA in the rupture model. The Nantou earthquake of 27 March 2013 is one of the well-recorded earthquakes in the strong motion network of Taiwan. The objective of this paper was to finalize the parameters of the rupture model of the Nantou earthquake by comparing the observed and simulated records using modified semi-empirical technique given by Joshi et al. (2014).

2 Geology and tectonic activity of Taiwan

Taiwan is located at boundary between the Philippine Sea plate to the East and the Eurasian plate to the West (Figs. 1, 2) with a convergence rate of 80 mm per year in the N118E direction (Seno 1977; Yu et al. 1997). This plate boundary is rather complex since

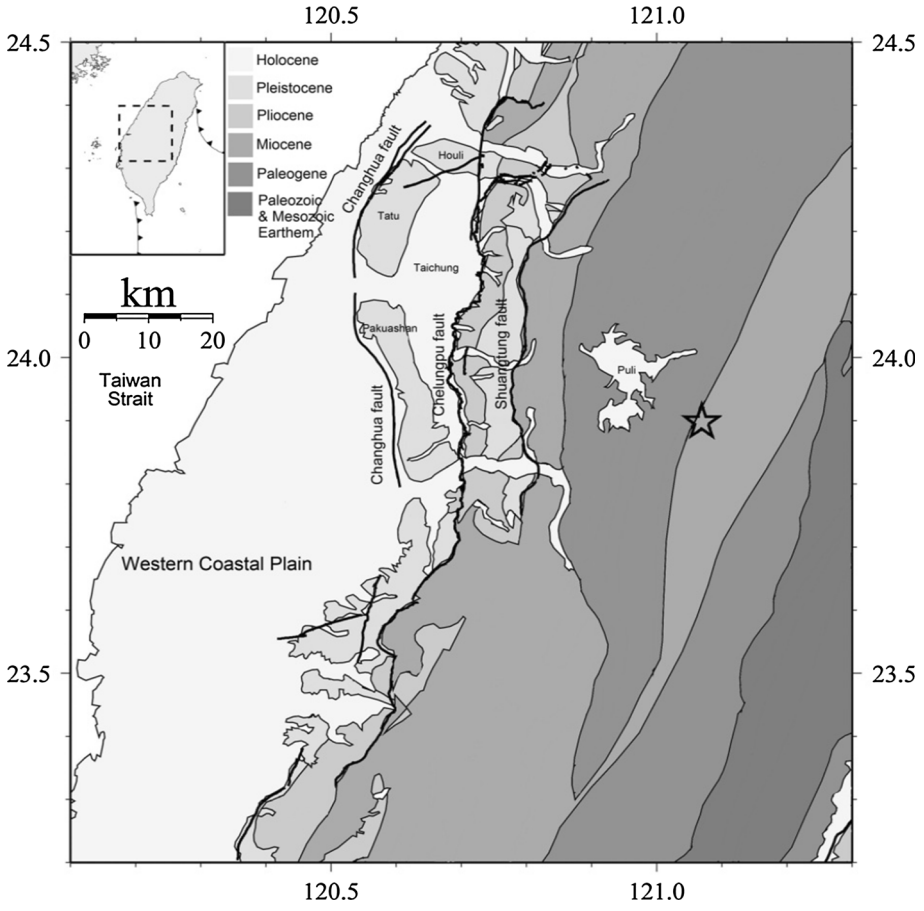

Fig. 1 Geological map of central Taiwan (CGS 2000) with active faults (Lin et al. 2008) and the epicentre of the 27 March 2013 Nantou earthquake

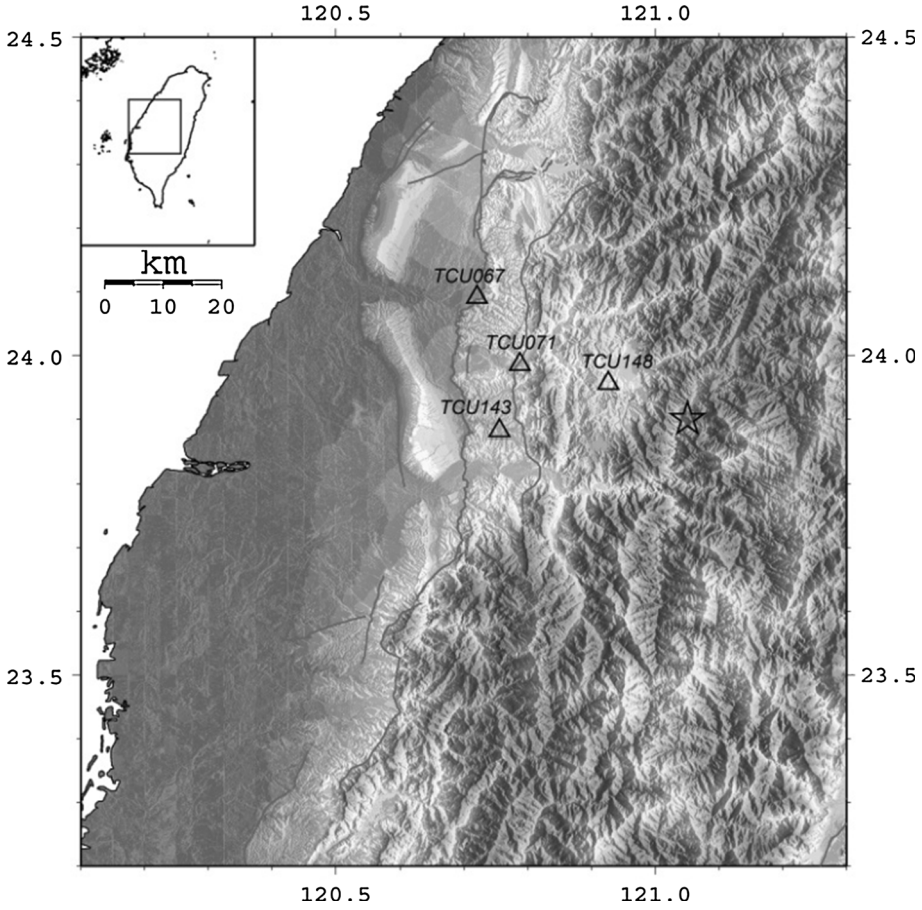

Fig. 2 Location of the recording stations used in this study as well as the epicentre of 27 March 2013 Nantou earthquake. *Star* shows the epicentre of this earthquake, and the *open triangles* show the station position of strong motion records used in the present work. This figure is plotted using Generic Mapping Tools (Wessel and Smith 1991)

it is comprised two subduction zone with reverse polarities. To the south-west is the ongoing subduction of the Eurasian plate eastward beneath the Philippine Sea plate along the Manila trench. The high-activity collisions between plates result in frequent earthquakes. The Nantou earthquake was located in the west seismic belt which is one of the three major seismic zones in Taiwan. Because the west seismic belt is very close to the metropolitans in western Taiwan several damaging earthquakes have occurred in this belt such as 1906 Meishan earthquake (M_L 7.1), 1935 Hsinchu–Taichung earthquake (M_L 7.1) and 1999 Chi–Chi earthquake (M_L 7.3, M_w 7.6). The Nantou earthquake was located in almost the centre of Taiwan Island. The epicentre was situated on the outcrop of the boundary between formations of Miocene and Oligocene (Fig. 1). The last earthquake in this region with a magnitude larger than 6 is the Mingjian earthquake (M_L 6.2) that occurred in 2009 (Lin et al. 2014), and then is the 1999 Chi–Chi earthquake sequence. Three N–S trending active thrust faults are placed at western foothills, called Changhua,

Chelungpu and Shuangtung fault, respectively. The eastern Shuangtung fault is the boundary between Miocene and Pleistocene (Toukoshan) formations. The Chelungpu fault is the boundary between Pliocene (Chinshui) and Holocene formations. The western Changhua fault thrusts Toukoshan Formation out to form gravel terraces and an elongated Holocene basin (Taichung) between itself and the Chelungpu fault. The Western Coastal Plain was filled with very thick Quaternary sediments covering order bedrocks. Under the Western Coastal Plain is a pre-Miocene basement, the Peikang Basement High, acts as a tectonic barrier and plays an important role for the seismogenic structure in middle of western Taiwan (Meng 1971; Lin et al. 2014).

3 Data

The Nantou earthquake of 27 March 2013 ($M_L = 6.24$ and $M_w = 5.9$) was recorded at 384 strong motion stations of Free-Field Taiwan Strong Motion Instrumentation Program (TSMIP) located within Taiwan (Liu et al. 1999). The seismic source parameters from US Geological Survey (USGS) and Harvard Centroid Moment Tensor (CMT) are shown in Table 1. This earthquake was recorded at the stations placed at the surface of earth which contain site amplification terms. The simulation technique given in this work is used for simulation of the strong motion record at the top of rock boundary without incorporating the soil effects. For comparing the observed records with the simulated records at the rock site, the transfer function is required to convert record at soil site into that at the rock site. The algorithm for transfer function is given by Idriss and Sun (1992) and is named as SHAKE91. This algorithm is modified version of the original program SHAKE (Schnabel et al. 1972) that is based on continuous solution to the wave equation for vertically propagating shear waves (Kanai 1951; Matthiesen et al. 1964; Roesset and Whitman 1969; Lysmer et al. 1971). The input to this algorithm requires record at rock site and the shear wave velocity profile of the soil layer.

The earthquake caused slight building damages in the Nantou County and Taichung City in the north-west from the epicentre within a distance of about 50 km, mainly tiles scaling off and RC wall cracking (NCREE 2013). According to the observation shake map from Central Weather Bureau (CWB), the north-western part suffered the strongest shaking during the earthquake and this shaking coincides with the distribution of damage. In order to simulate the strong ground motions at rock sites, stations recorded seismic intensity larger than 6 (peak ground acceleration larger than 250 gal) and also contain

Table 1 Parameters of March 27 2013 Nantou earthquake, Taiwan

Hypocentre	Size	Fault plane solution	Reference
March 27 2013 02:03:19.90 s UTC 23.850° N 121.22° E 19.4 km	$M_0 = 8.3 \times 10^{24}$ dyne cm $M_w = 5.9$	NP1 $\varphi = 24°$ $\delta = 23°$ NP2 $\varphi = 197°$ $\delta = 67°$	USGS
March 27 2013 02:03:21.5 GMT 23.91° N 120.84° E 22.7 km	$M_0 = 1.17 \times 10^{25}$ dyne cm $M_w = 6.0$ $m_b = 5.8$ Ms = 5.9	NP1 $\varphi = 359°$ $\delta = 24°$ $\lambda = 80$ NP2 $\varphi = 190°$ $\delta = 66°$ $\lambda = 94$	CMT (Harvard)

Table 2 Details of Vs30 at different stations

Station code	Coordinates	Vs30 (m/s)
TCU148	120.92, 23.95	513
TCU143	120.75, 23.88	465
TCU071	120.78, 23.98	614
TCU067	120.72, 24.09	440

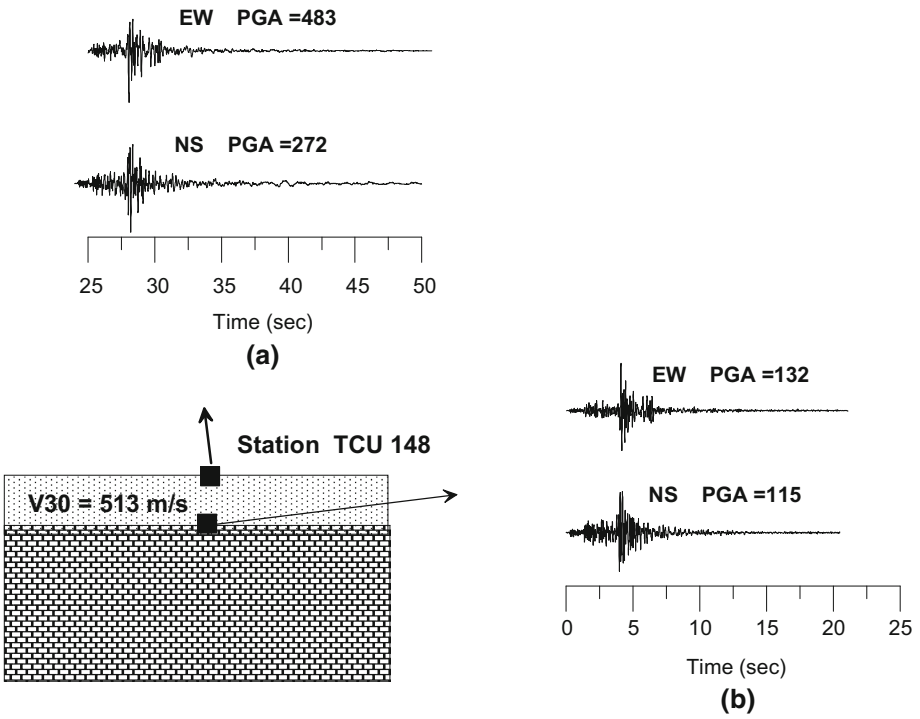

Fig. 3 Processed NS and EW components of observed strong motion acceleration of station TCU148 at **a** soil site and after using the SHAKE91 at **b** rock site are shown

logging velocity profiles in the shallow layer are required. Four stations were therefore selected for the simulation in this study under the criteria. The locations of selected stations (TCU067, TCU071, TCU143 and TCU148) and the epicentre of the Nantou earthquake are shown in Fig. 2. The digital data of accelerations used in this study were obtained from CWB's Geophysical Database Management System (Shin et al. 2013). In the present work, the Vs30 for each site (Kuo et al. 2012) given in Table 2 has been used. The observed records have been converted into that at the rock site using this velocity input. It is seen that the corrected observed records at all four sites show high amplitude at long periods which may be possibly from local site effects that remain still in the records after application of the transfer function. In order to remove long period high amplitudes from corrected records, these records have been filtered by applying a fourth-order Chebyshev filter of frequency range 2.5–25 Hz. The processed filtered observed records at the rock sites using transfer function are shown in Figs. 3, 4, 5 and 6. Peak ground acceleration

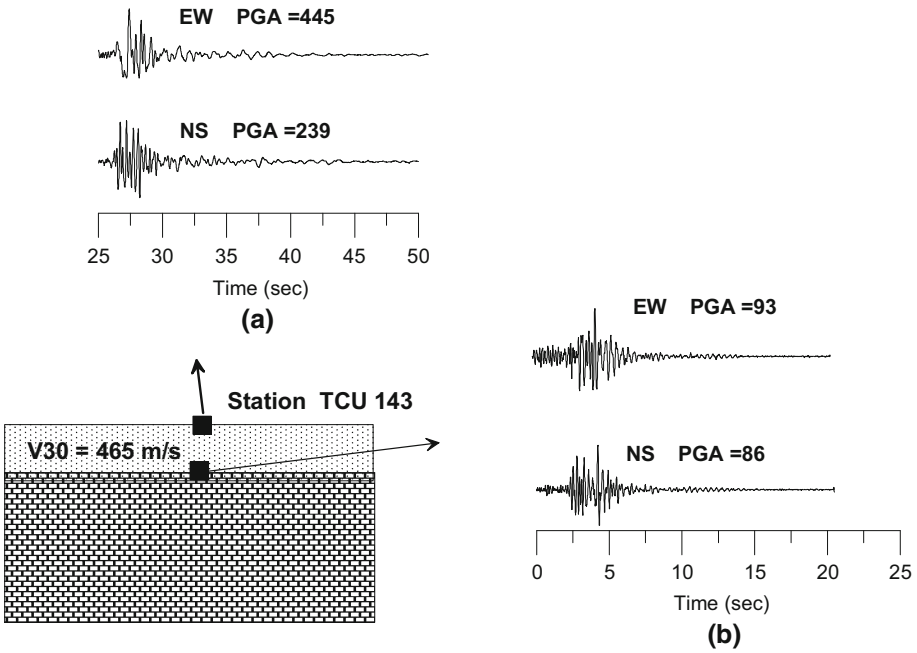

Fig. 4 Processed NS and EW components of observed strong motion acceleration of station TCU143 at **a** soil site and after using the SHAKE91 at **b** rock site are shown

values at these stations are shown in Table 3. These records are further used for comparison with simulated records. In the present work, simulated records are also filtered in the same range as used in the processing of observed records.

The method of simulation presented in this paper is based on division of the rupture plane of the target earthquake into subfaults. This division is based on self-similarity laws given by Kanamori and Anderson (1975). The division is strongly dependent on the source parameters of the earthquake used as subfault to model the target earthquake. These source parameters include seismic moment and stress drop of the target and subfault events. In the present work, the rupture plane of the Nantou earthquake has been subdivided into several subfaults on the basis of the parameters of one of the aftershocks of this earthquake. Parameters of this aftershock are given in Table 4. Calculation of the source parameter requires full waveform data. In the present work, waveform data of the mainshock and the aftershock recorded at TCU148 station have been used. Detail of this station is given in Table 4. Location of the mainshock event as well as that of the recording station is shown in Fig. 2.

The source displacement spectrum of mainshock and aftershock is obtained after correcting the shear wave spectrum of the displacement record for anelastic attenuation and geometrical spreading term (Table 5).

The anelastic attenuation term requires knowledge of shear wave quality factor. In the present work, shear wave quality factor given by Sokolov et al. (2009) has been used for obtaining source displacement term. The source displacement spectra of the mainshock and aftershock from both horizontal components are shown in Fig. 7. The long-term flat level Ω_o and corner frequency 'f_c' are two important parameters that are extracted from source displacement spectra. These two parameters are directly used in various formulas to obtain

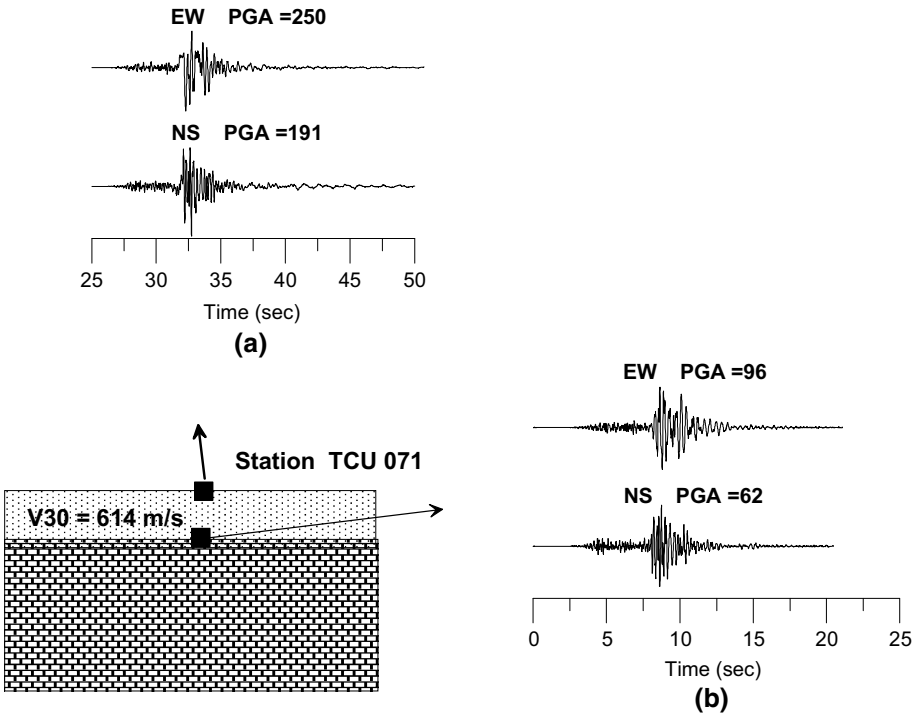

Fig. 5 Processed NS and EW components of observed strong motion acceleration of station TCU071 at **a** soil site and after using the SHAKE91 at **b** rock site are shown

seismic moment and stress drop. Seismic moment (M_0) can be calculated from knowledge of long-term flat level by using following formula given by Brune (1970, 1971):

$$M_0 = 4\pi\rho\beta^3\Omega_0 R/\mathrm{FS} \times R_{\theta\varphi} \times \mathrm{PRIT} \quad (1)$$

where ρ and β are the density and the S-wave velocity of the medium, respectively, FS is the free-surface effect, Ω_o is the long-term flat level of the source displacement spectrum at a hypocentral distance of R, PRIT is factor that accounts partitioning of energy into two horizontal component and $R_{\theta\varphi}$ is the radiation pattern coefficient of S phase. We have used the value of density and shear wave velocity as 2.8 gm/cm^3 and 2.9 km/s, respectively. The shear wave velocity used in this work is an average of velocities in various layers above 19 km in the velocity section given by Ho (1994). The radiation pattern coefficient $R_{\theta\varphi}$, FS and PRIT have been approximately taken as 0.55, 2.0 and .71 for S-wave, respectively (Atkinson and Boore 1995). One of the important parameters of an earthquake source is the stress drop ($\Delta\sigma$), which is defined as the difference of pre-existing tectonic stress and the dynamical frictional stress. For a circular crack of radius 'r_0', the stress drop '$\Delta\sigma$' is given as (Papageorgiou and Aki 1983):

$$\Delta\sigma = 7M_0/16r_0^3 \quad (2)$$

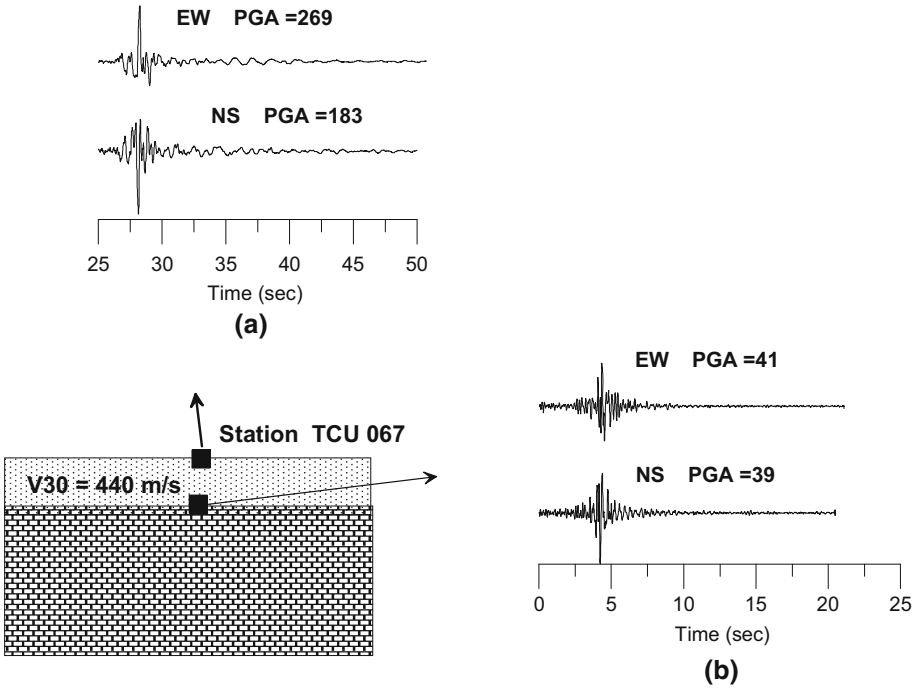

Fig. 6 Processed NS and EW components of observed strong motion acceleration of station TCU067 at **a** soil site and after using the SHAKE91 at **b** rock site are shown

The corner frequency 'f_c' of the source displacement spectra is related to the radius 'r_0' of the equivalent circular crack, which is used to model the earthquake. The relation between 'r_0' and the corner frequency 'f_c' is given as (Brune 1970, 1971):

$$r_0 = 2.34\beta/2\pi f_c \tag{3}$$

Parameters of the mainshock and the aftershock computed from source displacement spectra are given in Table 6. It is seen that average seismic moment of the mainshock is 3.4×10^{24} dyne cm which is quite close to the value reported by USGS and CMT Harvard. However, in the present work, the initial value of seismic moment and other parameters have been fixed using earthquake parameters given by CMT Harvard.

4 Methodology

The technique of semi-empirical simulation used in this paper is that initially developed by Midorikawa (1993) and later modified by Joshi (2004), Joshi and Midorikawa (2004), Joshi and Mohan (2008) and Joshi et al. (2012a, b, 2014). The first part of this technique deals with simulation of a time series having basic spectral shape of accelerogram, while the second part deals with simulation of envelope due to the deterministic model of rupture plane. The modified semi-empirical method uses the time series obtained from stochastic simulation technique and envelope function obtained from the semi-empirical approach to simulating strong ground motion at the observation point. In the stochastic simulation

Table 3 Filtered peak ground acceleration value from observed records at the rock site

Station code	PGA (NS) (gal)	PGA (EW) (gal)
TCU148	115	132
TCU143	86	93
TCU071	62	96
TCU067	39	41

Table 4 Detail of the strong motion recording station which has recorded the Nantou earthquake

Station name	Latitude (in degree)	Longitude (in degree)	Station code
TCU148	23.956	120.926	TCU148

technique, the white Gaussian noise of zero expected mean and variance chosen to give unit spectral amplitude has been passed through number of filters representing the earthquake processes. The shape of acceleration spectra $A(f)$ at a site of simulation located at an hypocentral distance R is given as (Boore 1983):

$$A(f) = CS(f)D_S(f)F_R(f,R) \tag{4}$$

where C is a scaling factor which is constant for given site and is given by (Boore 1983):

$$C = M_0 \cdot R_{\theta\varphi} \cdot FS \cdot PRTITN / 4\pi\rho\beta^3 \tag{5}$$

In this expression, M_0 is the seismic moment, $R_{\theta\varphi}$ is the radiation pattern, FS is the amplification due to the free surface, $PRTITN$ is the reduction factor that accounts for the partitioning of total shear wave energy into two horizontal components (taken as $1/\sqrt{2}$), and ρ and β are the density and shear velocity, respectively. The radiation pattern $R_{\theta\varphi}$ is dependent on the type of faulting mechanism and the geometry of earthquake source and is calculated by using the formulation given by Aki and Richards (2002). The filter $S(f)$ in Eq. (1) is the source acceleration spectrum and is defined as follows (Brune 1970):

$$S(f) = (2\pi f)^2 \Big/ \left[1 + (f/f_c)^2\right] \tag{6}$$

The filter $D_S(f)$ used in Eq. (4) is the near-site attenuation of high frequencies and is defined as (Boore 1983):

$$D_S(f) = 1 \Big/ \left[1 + (f/f_m)^8\right]^{1/2} \tag{7}$$

The parameter f_m represents the high-frequency cut-off range of the high-cut filter. The filter $F_R(f, R)$ in Eq. (4) represents the effect of anelastic attenuation and is given as (Boore 1983):

$$F_R(f,R) = \left(e^{-\pi f R / \beta Q_\beta(f)}\right) \Big/ R \tag{8}$$

In this expression, R denotes the hypocentral distance in km and $Q_\beta(f)$ is the quality factor which defines the frequency-dependent attenuation of shear waves. In the present work, the

Table 5 Parameters of the aftershock of 27 March 2013 Nantou earthquake, Taiwan

Origin time	Hypocenter	Size
03:30 UTC 14.02 km	23.93°N 121.0°E	$M_L = 4.54$

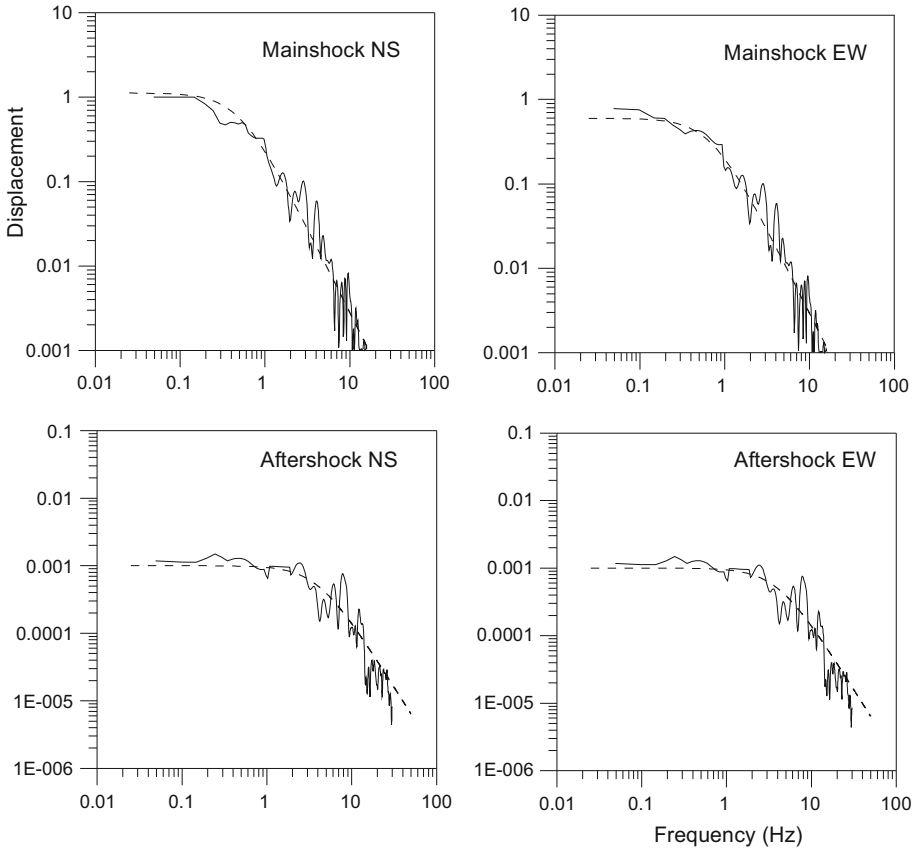

Fig. 7 Displacement spectra of recorded S phase of mainshock and aftershock acceleration record along with their theoretical spectra (in *dashed line*) for NS and EW component of the Nantou earthquake at TCU148 station

frequency-dependent quality factor $Q_\beta(f)$ for the Taiwan region given by Sokolov et al. (2009) has been used as $Q_\beta(f) = 80f^{0.9}$. The spectrum of white noise after multiplication with theoretical filters given in Eq. (4) represents basic shape of acceleration spectra due to an earthquake. Time domain representation of this acceleration spectrum gives an acceleration record that has basic properties of acceleration spectra. However, this time domain representation of acceleration record raises serious problem, like the obtained records overestimate the high frequency and underestimate low frequency in the synthetic strong ground motion. This is due to the difference in duration of slip of the target and the small earthquake

Table 6 Ground motion parameters of the mainshock and the aftershock of the Nantou earthquake estimated from displacement spectra

Parameters	Hypocentral distance (km)	Long-term flat level, Ω_0 (cm-s)	Corner frequency, f_c (Hz)	Seismic moment, M_0 (dyne cm)	$\Delta\sigma$ (bars)
Mainshock NS	38	1.00	0.5	4.2×10^{24}	181
Main shock EW	38	0.6	0.7	2.5×10^{24}	298
Aftershock NS	16	0.001	4	1.8×10^{21}	39
Aftershock EW	16	0.001	4	1.8×10^{21}	39

considered as subfaults. The difference in the duration of slip of the target and the subfault earthquake can be calculated by convolving the obtained records with the correction function $F(t)$ given by Irikura et al. (1997) and Irikura and Kamae (1994). The convolution of $F(t)$ with obtained acceleration record $a_{ij}(t)$ gives acceleration record $A_{ij}(t)$ as:

$$A_{ij}(t) = F(t) * a_{ij}(t) \tag{9}$$

where i and j represent the position of subfault along the length and the width of the rupture plane, respectively. It is observed that stochastic simulation technique requires proper windowing of the obtained record by a function which should preferable based on the kinematic representation of model of rupture plane (Boore 1983). In the present work, such time window can be obtained by the semi-empirical technique of Midorikawa (1993) in the form of resultant envelope of accelerogram obtained from a model of finite rupture plane.

The resultant envelope at the observation point using semi-empirical approach is calculated by dividing the rupture of the target earthquake into several subfaults. The division of rupture plane of the target events into subfaults is based on the self-similarity laws proposed by Kanamori and Anderson (1975). Each subfault releases energy whenever rupture front reaches centre of subfaults. The energy is released in the form of acceleration envelope. The acceleration envelope $e_{ij}(t)$ is determined from the following functional form given by Kameda and Sugito (1978) and further modified by Joshi (2004):

$$e_{ij}(t) = T_{ss}(t/T_d) \cdot \exp(1 - t/T_d) \tag{10}$$

In this expression, T_d represents duration parameter and T_{ss} represents the transmission coefficient of incident shear waves. This coefficient is given by the following formula after Lay and Wallace (1995, p. 102) and is used by Joshi et al. (2001) for modelling the effect of the transmission of energy in the shape of acceleration envelope. The transmission coefficient contributes significantly to shaping the attenuation rate of the peak ground acceleration with respect to the distance from the source. Joshi and Midorikawa (2004) have observed that for the shallow focus earthquakes, the transmission coefficient is ≈ 1.0; however, for the intermediate to deep focus earthquake, this coefficient is $\neq 1.0$. This means that we should take this coefficient into consideration when modelling an intermediate to deep focus earthquake.

The parameters required to define the model of the rupture plane are its length (L), width (W), length and width of the subfaults (L_e, W_e), nucleation point, strike, dip and rake of rupture plane (φ_s, δ, λ), rupture velocity (V_r) and shear wave velocity in the medium. The rectangular rupture plane of a target earthquake of seismic moment M_0 is divided into $N \times N$ subfaults of seismic moment M_0. Once the rupture plane of target earthquake is divided into subfaults, one subfault is fixed as nucleation point from which the rupture

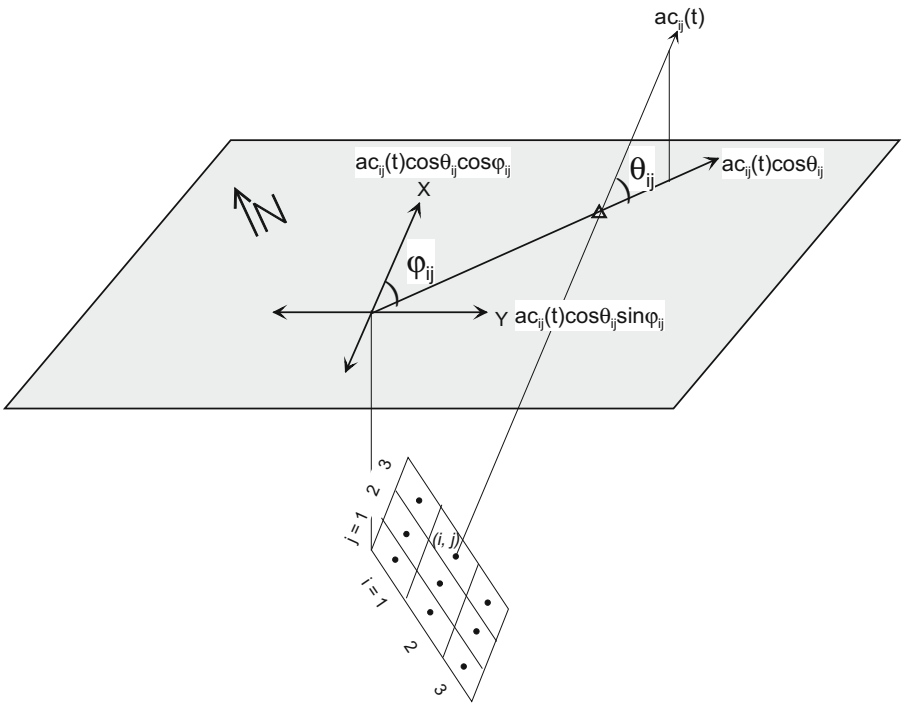

Fig. 8 Illustration of method for simulation of NS and EW component of earthquake ground motion from '*ijth*' subfault. *Triangle* shows the recording station

initiates. The rupture starts from the nucleation point and propagates radially within the rupture plane. The subfault releases energy whenever the rupture front touches its centre. The energy is released in the form of the acceleration record $ac_{ij}(t)$, which is the product of acceleration record from stochastic technique with the envelope function from semi-empirical technique. This can be given as:

$$ac_{ij}(t) = e_{ij}(t) \cdot A_{ij}(t) \tag{11}$$

The acceleration record, $ac_{ij}(t)$, released from different subfaults reaches the observation point at different time lags. The arrival time at the observation point 't_{ij}' depends on the time taken by rupture from nucleation point to *ij*th subfault with rupture velocity V_r and the time taken by energy released from *ij*th subfault to reach the observation point with shear wave velocity. Simple vector notation has been used to resolve the resultant component into horizontal components. The direction of resultant component from each subfault is defined by a line joining centre of subfault to the recording station. This direction is different for different subfaults and for obtaining horizontal component along strike and perpendicular direction of the modelled rupture plane; records from each subfault need separate treatment. Figure 8 shows the division of total acceleration record ac_{ij} (t) into components along strike and dip directions. Following formula is used for obtaining horizontal component of records along the direction of strike (X axis) and the direction of dip (Y axis) of the modelled fault, respectively, from resultant component $ac_{ij}(t)$ released by *ij*th sub-fault. The acceleration components along X and Y directions are represented by $ac_{ij}^{X}(t)$ and $ac_{ij}^{Y}(t)$ and are defined as follows:

$$ac_{ij}^{X}(t) = ac_{ij}(t) \cdot \cos\theta_{ij} \cdot \cos\varphi_{ij} \tag{12}$$

$$ac_{ij}^{Y}(t) = ac_{ij}(t) \cdot \cos\theta_{ij} \cdot \sin\varphi_{ij} \tag{13}$$

In Eqs. (12) and (13), φ_{ij} represents the angle made by horizontal projection of resultant ground acceleration from ijth sub-fault with the direction of strike of the modelled fault and θ_{ij} represents the angle made by resultant ground acceleration with the vertical. The angles θ_{ij} and φ_{ij} are different for different sub-faults and depend on the position of sub-fault within the rupture plane. Once the components of acceleration records are obtained along X and Y axis for ground acceleration released from each sub-faults, it is further rotated by angle $\emptyset$ using following matrix rotation formula to obtain component along NS and EW direction:

$$\begin{bmatrix} ac_{ij}^{NS} \\ ac_{ij}^{EW} \end{bmatrix} = \begin{bmatrix} \cos\phi & -\sin\phi \\ \sin\phi & \cos\phi \end{bmatrix} \begin{bmatrix} ac_{ij}^{X}(t) \\ ac_{ij}^{Y}(t) \end{bmatrix} \tag{14}$$

where ac_{ij}^{NS} and ac_{ij}^{EW} are the components of acceleration record along NS and EW direction, respectively, and $\emptyset$ is the strike of the modelled rupture plane measured with respect to the geographic north. Summation of all NS and EW components of acceleration record released from different subfaults reaching the observation point at different time lag t_{ij} gives the final NS and EW components of acceleration record as follows:

$$Ac^{NS}(t) = \sum_{i=1}^{N}\sum_{j=1}^{N} ac_{ij}^{NS}\left(t - t_{ij}\right) \tag{15}$$

$$Ac^{EW}(t) = \sum_{i=1}^{N}\sum_{j=1}^{N} ac_{ij}^{EW}\left(t - t_{ij}\right) \tag{16}$$

where $Ac^{NS}(t)$ and $Ac^{EW}(t)$ represent the north–south and east–west component of acceleration records, respectively.

5 Rupture model of the Nantou earthquake

The rupture length and width of the Nantou earthquake have been considered as 40 and 25 km, respectively, by Lee (2013). The seismic moment of the mainshock and the aftershock of the Nantou earthquake and ratio of stress drop have been used for dividing the rupture plane of the target earthquake into various subfaults. Average value of seismic moment of the aftershock and stress drop ratio of target and subfault events has been used for division of rupture plane into subfaults. Although the entire rupture area can be modelled for strong motion generation, it is seen that the duration obtained by modelling entire rupture plane is very high which clearly ruled out observation which is supported by less duration of strong motion record. Visual inspection of records of this earthquake clearly shows that duration of high-frequency ground motion is certainly less than expected. The duration of strong motion shaking observed from one of the near-field station like TCU148 contain total duration of about 4.96 s. Considering maximum speed of rupture propagation as 3.04 km/s within the length of 40 km the total duration of strong motion record should be approximately equal or more than 13.0 s. Clear deviation from observed and theoretically possible duration from rupture model clearly shows that the

Table 7 Initial parameters of the SMGA of the Nantou earthquake, Taiwan, used for simulation

Modelling parameter	Source
Length = 5 km	
Width = 5 km	
Dip = 24°	CMT Harvard
Strike = 359°	CMT Harvard
Rake = 80°	CMT Harvard
$N_L = 10$	Based on scaling relation by Kanamori and Anderson (1975)
$N_W = 10$	Mendoza and Hartzell (1988)
$V_r = 2.32$ km/s	
Stress drop ratio = 6.1	Calculated from displacement spectra
Seismic moment of subfault = 1.8×10^{21} dyne cm	Calculated from self-similarity laws
$\beta = 2.9$ km/s	Average value from velocity section
$Q_\beta(f) = 80f^{0.9}$	Sokolov et al. (2009)
SPR = (10.2)	Initial Guess

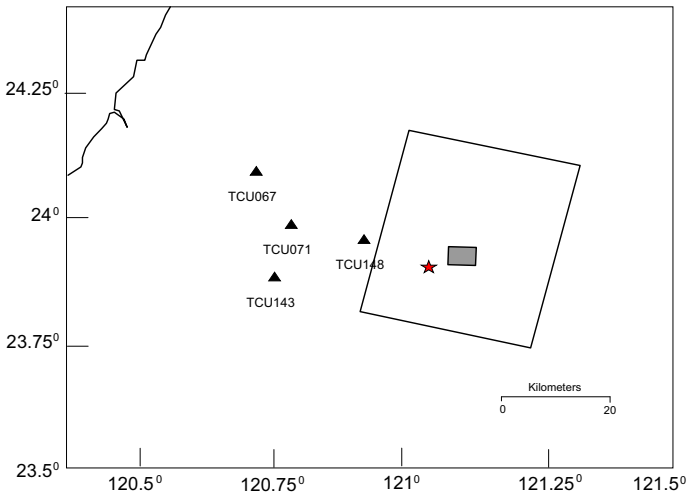

Fig. 9 Location of the SMGA of the Nantou earthquake of magnitude (M_w) 5.9. *Triangles* show the position of strong motion stations used in this study. The *star* shows the epicentre of the earthquake. The *solid rectangle* shows the SMGA of the Nantou earthquake, while *empty rectangle* shows rupture responsible for the Nantou earthquake

strong motion generation area is somewhat less than the total rupture area responsible for this earthquake. It is seen that the high slip area of this rupture model is very small which also supports idea of SMGA. In the present work, an area of size 5 km × 5 km has been modelled as SMGA and same has been assumed as strong motion generation area in the present approach. Parameters of the modelled SMGA within the rupture plane responsible for the Nantou earthquake are listed in Table 7. The location of the rupture plane and the

Table 8 Velocity model (after Ho 1994)

Depth (km)	*P*-wave velocity (km/s)	S-wave velocity (km/s)
0.0	3.50	2.00
1.0	3.78	2.20
4.0	5.04	3.03
9.0	5.71	3.26
13.0	6.05	3.47
17.0	6.44	3.72
25.0	6.83	3.99
30.0	7.28	4.21

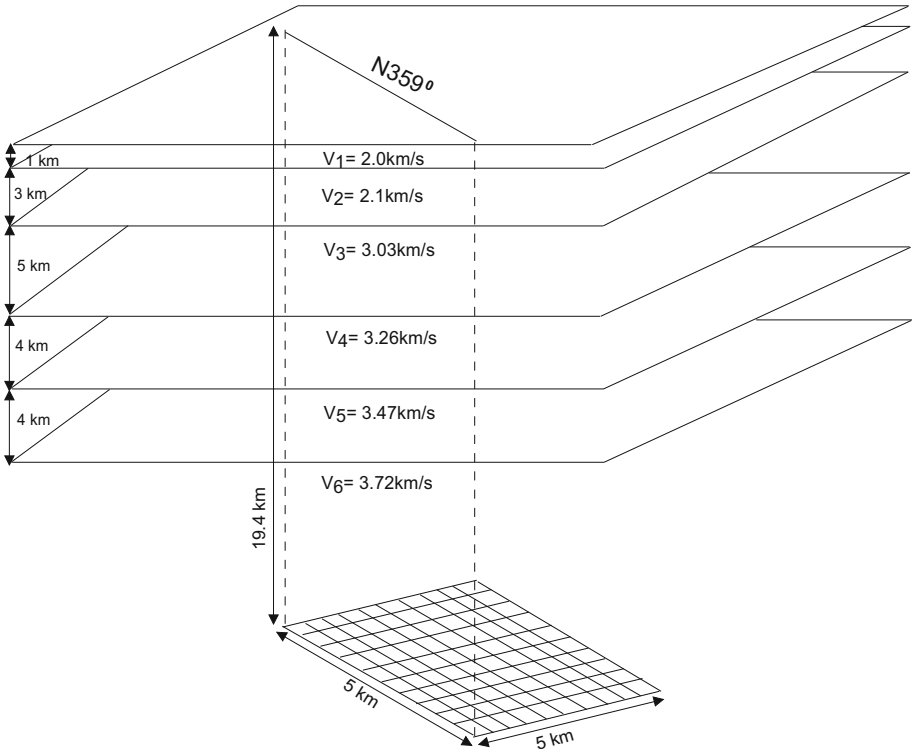

Fig. 10 Model of SMGA of the Nantou earthquake consisting 10 × 10 subfaults placed in a layered medium with 359°N strike direction. The velocity of medium is defined by Ho (1994)

SMGA is shown in Fig. 9. The strike and dip of this SMGA are decided on the basis of fault plane solution given by CMT Harvard and are given in Table 7. The velocity model that has been used for simulation of strong ground motion is given by Ho (1994) and is given in Table 8. The rupture plane of the target earthquake for purpose of modelling is placed in the sixth layer of velocity model at a depth of 19.4 km and is shown in Fig. 10. Based on self-similarity laws and the earthquake parameters of target events given by CMT Harvard, SMGA is divided into 10 × 10 subfaults. The ratio of average stress drop of

target and subfault earthquake is 6.1. The rupture velocity of 2.32 km/s has been calculated using the criteria of Mendoza and Hartzell (1988) which define rupture velocity to be 80 % of shear wave velocity.

6 Model selections

It is seen that the strong motion simulations are influenced by several parameters of the rupture plane. Once initial model has been decided, then the next task is to finalize the parameters of final rupture plane. Judgement of the best model is based on root mean square error (RMSE) of peak ground acceleration at all four stations. Therefore, each model has been tested to calculate peak ground acceleration values of NS and EW components at each four stations. Following formula has been used to calculate RMSE of peak ground acceleration parameter

$$\mathrm{RMSE} = (1/N) \cdot \left[\Sigma(a_0 - a_s)^2\right]^{1/2}$$

where a_0 and a_s are accelerations of observation and simulation at times, respectively. The parameter N represents total peak ground acceleration values.

In the present work, various modelling parameters such as dip, strike, rake and starting points of rupture are changed iteratively in a specified range in a heuristic way to obtain best modelling parameters. Table 9 gives the range of parameters that are considered for final model.

Several records at all four stations have been simulated to check the dependency of simulated records on various modelling parameters. It is seen that variation of different parameters effects simulated records significantly. Although initial guess about many parameters can be made from other independent studies, it is always better to finalize parameters of the rupture plane by iterative modelling and comparison with the observed data. In the present study, several simulations clearly indicate effect of dip, strike, rake and starting point of rupture in the simulated record. These parameters significantly affect the radiation pattern at the point of observation, thereby affecting the amplitude of acceleration at that point. The initial model of rupture plane is based on the earthquake parameters of main shock given by CMT Harvard, and other parameters are given in Table 7.

Dip of the rupture plane affects the arrival time of envelopes at the observation point and also the radiation pattern. For finalizing the amount of dip, 30 different models have been considered in a range of 20°–40° keeping other parameters similar as given in Table 7. Visual inspection of RMSE curve in Fig. 11 shows that minimum RMSE is obtained around 34°. Thirty new models have been also prepared for dip within a range of 32°–36°. It is seen from Fig. 11b that minimum RMSE is obtained at dip value of 34.13°.

Table 9 Range of modelling parameters

Model parameter	Range
Dip	20°–40°
Strike	N355°–N70°
Rake	75°–85°
Starting point of rupture	All elements

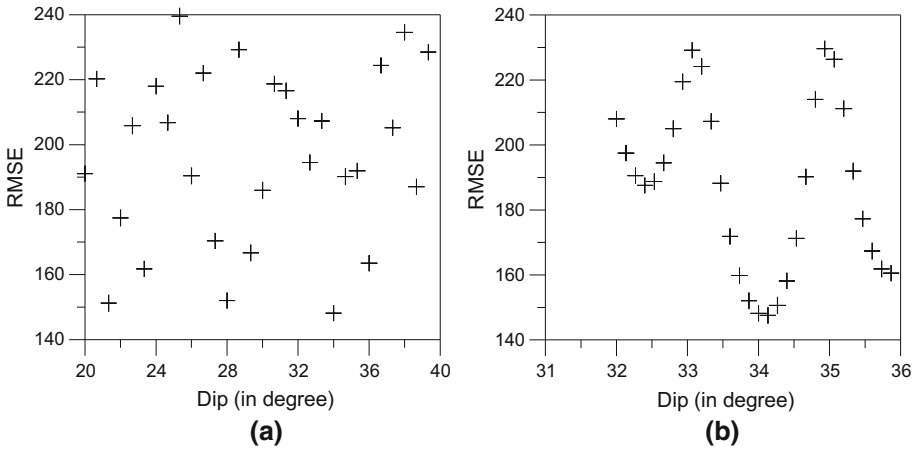

Fig. 11 Selection of dip

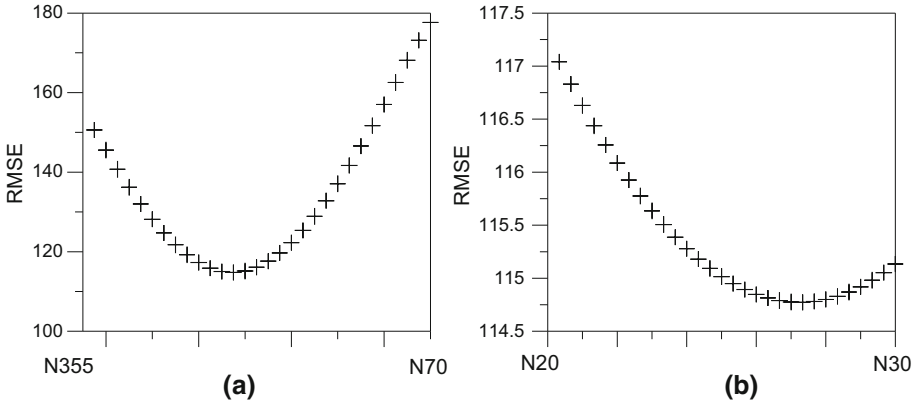

Fig. 12 Selection of strike

The strike of the rupture plane affects the arrival time of envelop at the observation point and the radiation pattern at the observation point. Thirty different rupture models in a range of N355°–N70° have been considered in this work with dip as 34.13°. Records were simulated at four stations, and RMSE has been calculated. The plot of RMSE with respect to the strike value in Fig. 12a shows a smooth variation of error with respect to dip amount with minimum value between N20° and N30°. On further examining thirty models within this range having uniform incremental difference in Fig. 12b, it is found that minimum RMSE is obtained at N27.3°.

In the present work, keeping all parameters same as reported in Table 7, several rupture models are prepared by changing rake in a range of 75°–85°. The dip and strike in these models are same as finalized earlier. Thirty different models shown in Fig. 13a have been considered in this work within a range of 75°–85°. Unlike strike of the rupture plane,

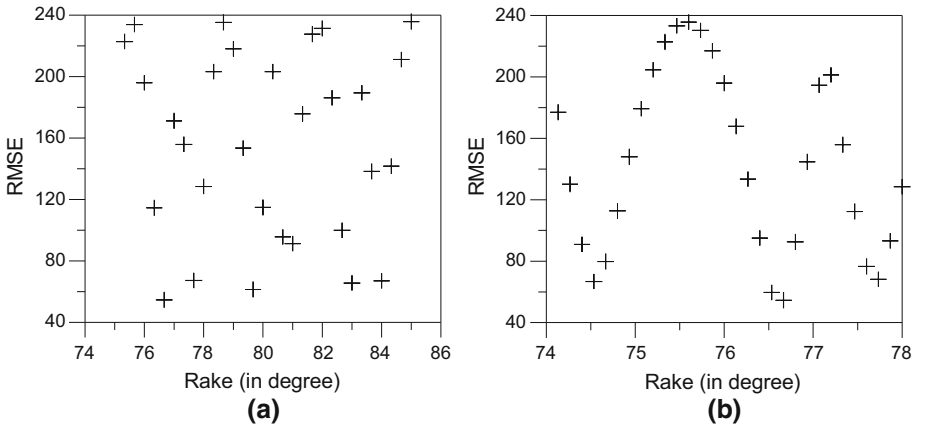

Fig. 13 Selection of rake

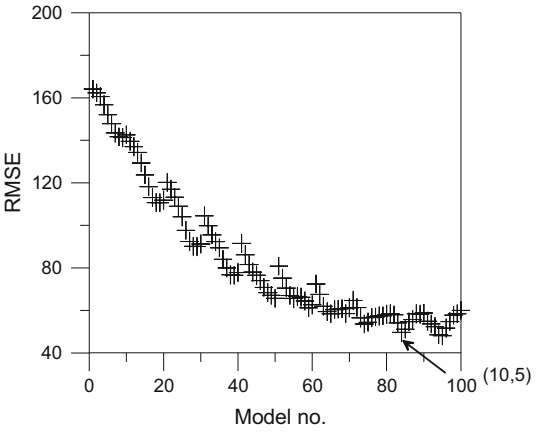

Fig. 14 Selection of starting point of rupture

Table 10 Final model

Model parameter	Range
Dip	34.13°
Strike	N27.3°
Rake	76.66°
Starting point of rupture	(10.5)

Table 11 Peak ground acceleration values from filtered simulated record at rock site. The values in parenthesis are the PGA value obtained from filtered processed actual records

Station code	PGA (NS) (gal)	PGA (EW) (gal)
TCU148	72 (115)	91 (132)
TCU143	38 (86)	48 (93)
TCU071	52 (62)	63 (96)
TCU067	50 (39)	40 (41)

dependency of RMSE in rake value is not so simple. It is seen from Fig. 13a that minimum RMSE is observed in a close range of 74°–78°. Thirty new models have been further

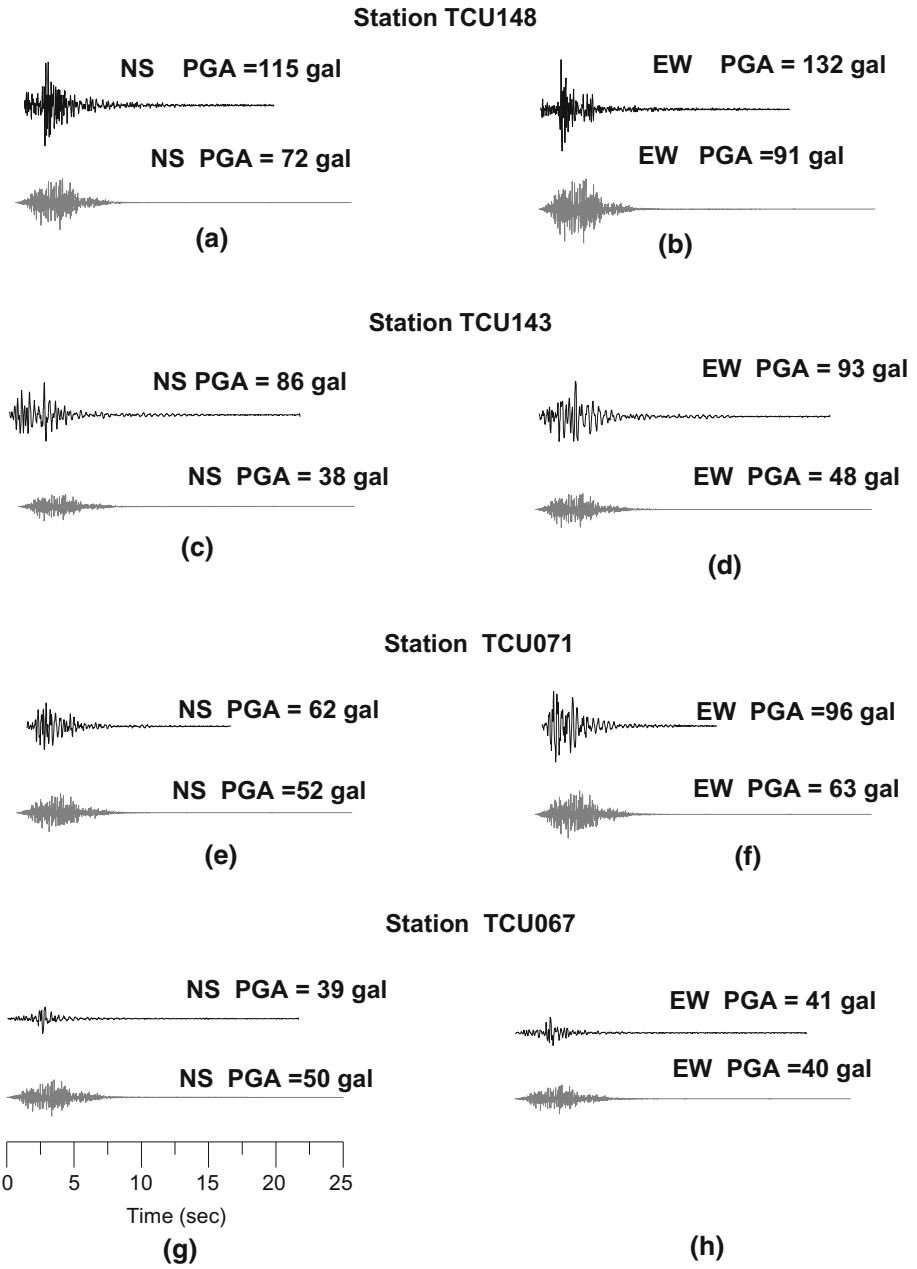

Fig. 15 Comparison of NS and EW components of observed and simulated strong motion acceleration records at various stations. *Black colour* represents the observed records and *grey colour* represents the simulated records, respectively

considered within this new range among which a minimum RMSE value at the rake of 76.66° has been observed as shown in Fig. 13b.

In any rupture model, possibilities of starting point of rupture are same as the number of subfaults within the rupture model. In the present work, each of 100 subfaults is considered as nucleation point, thereby giving rise to 100 different models having dip, strike and rake values finalized earlier. Root mean square error of peak ground acceleration at each station has been calculated from each model, and it is shown in Fig. 14 that minimum RMSE is

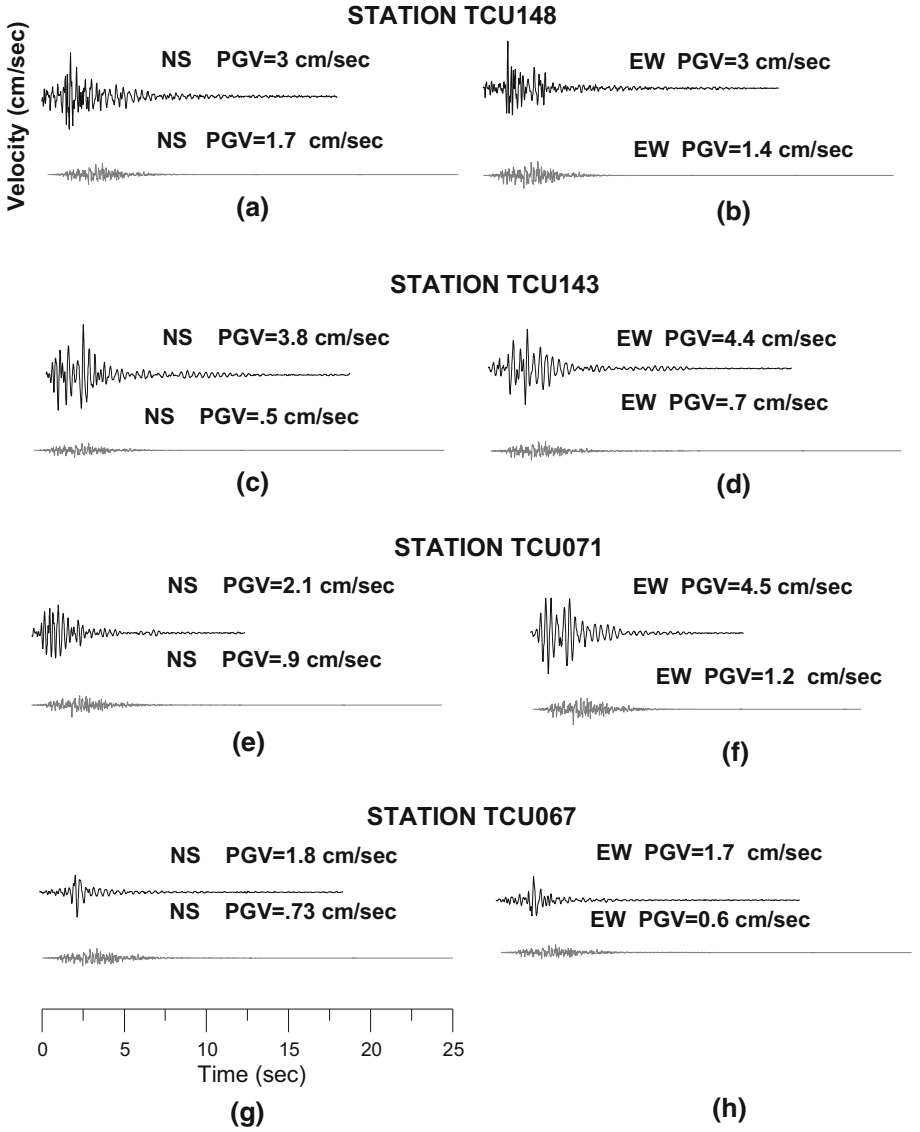

Fig. 16 Comparison of NS and EW components of observed and simulated velocity records at various stations. *Black colour* represents the observed records and *grey colour* represents the simulated records, respectively

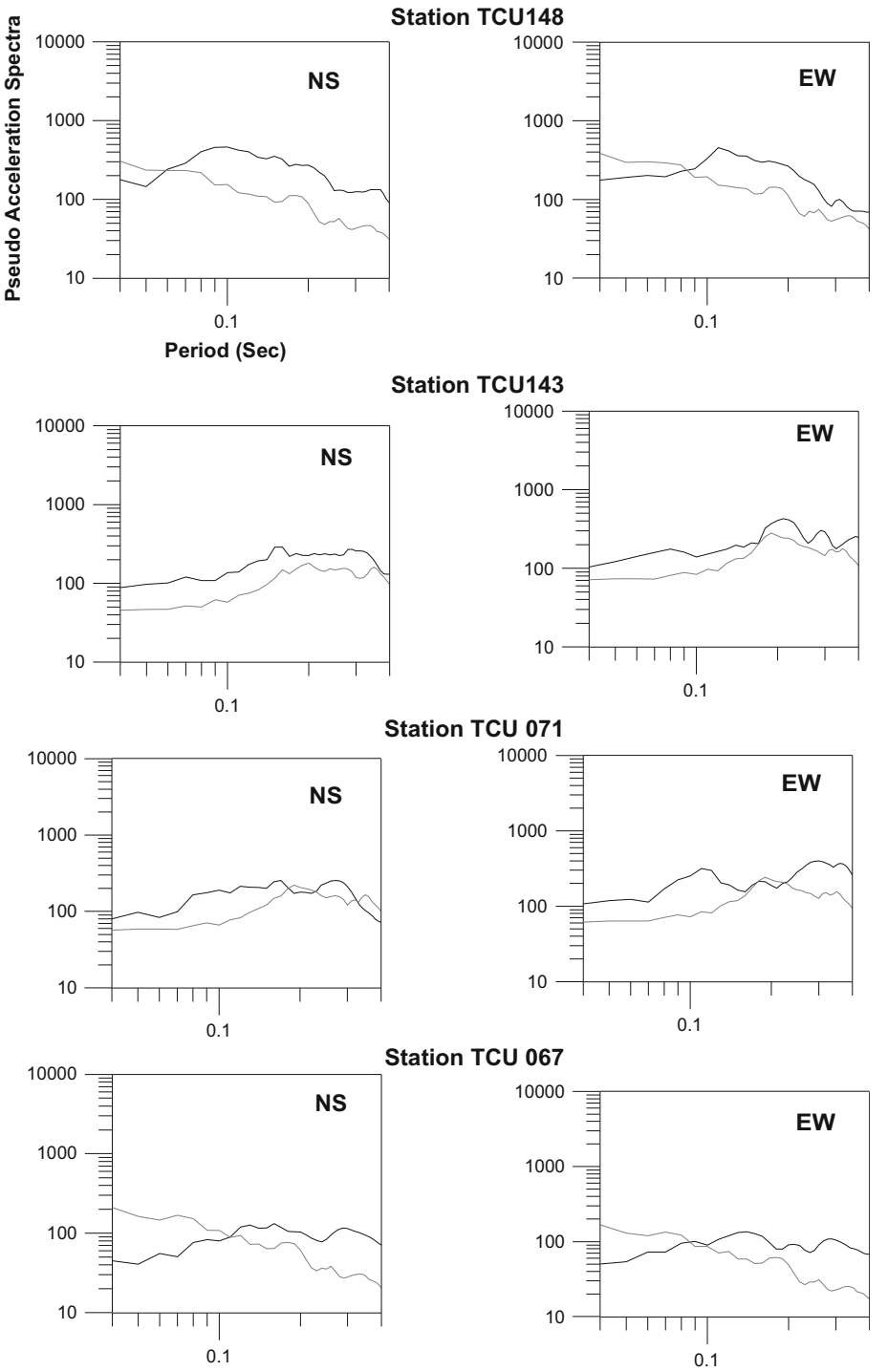
Station TCU148
Pseudo Acceleration Spectra
NS
EW
10000
1000
100
10
0.1
Period (Sec)
Station TCU143
NS
EW
Station TCU 071
NS
EW
Station TCU 067
NS
EW

◀**Fig. 17** Comparison of response spectra obtained from simulated and observed NS and EW component of strong motion response spectra records at various stations. *Black colour* represents the observed records and *grey colour* represents the simulated records, respectively

obtained for a case when nucleation point is at (10,5). Several simulations and RMSE computations give a final model of rupture plane given in Table 10.

7 Simulation of strong ground motion records of the Nantou earthquake, Taiwan

Once the rupture model has been finalized, the simulated records at four stations have been compared in terms of waveform and its parameters with the observed record. In order to remove long period undulations in the simulated strong motion records, Chebyshev filter of order 4 has been applied in a range of 2.5–25 Hz. The filtered simulated records at rock site have been compared with the filtered observed records converted at rock site. The value of peak ground acceleration at rock site obtained from both simulated and processed observed records is shown in Table 11.

Strong motion records indicate the presence of comparable match in the observed and simulated records. The simulation and observed records are shown in component wise in NS and EW. The response spectra of the simulated record give a comparable match from 0.04 to 0.4 s, respectively, almost for all stations. The records have been compared in terms of complete waveform. The simulated acceleration waveform at rock site is compared with the corrected acceleration at rock site and is shown in Fig. 15. The portion of corrected record after arrival of S phase has been used for comparison with the simulated records. It is seen that at all four stations the value of peak ground acceleration from observed and the simulated records is close to each other. The records match effectively in terms of its shape and statistical characteristics. The duration of corrected and simulated strong motion records also matches with each other. Simulated and corrected acceleration records are integrated to obtain velocity and displacement records. The velocity waveforms are obtained from integration of simulated and corrected acceleration records and are shown in Fig. 16. The waveforms of velocity records also confirm the validity of technique in effectively simulating record that bears realistic appearance in acceleration and velocity waveforms. The validity of any simulation technique can be judged by its ability to produce response spectra that matches with observed records. The response spectra at 5 % damping have been calculated from both simulated and corrected observed records and are shown in Fig. 17. It is seen that the response spectra from simulated and observed records also bear close resemblance with each other in frequency range 2.5–25 Hz, thereby establishing the efficacy of approach to simulating strong ground motion.

8 Conclusions

This paper uses modified semi-empirical technique (MSET) for simulation of strong ground motion. The simulation technique presented in this paper is based on the technique given by Midorikawa (1993). The modified technique has been used for simulation of the strong ground records of the Nantou earthquake ($M_w = 5.9$) of March 27 2013. The observed records have been converted into rock site using transfer function. The corrected observed records are used for comparison with simulated records at rock site. The modified

semi-empirical technique has been used to simulate horizontal components of strong motion records from several models having single strong motion generation area. Comparison of peak ground acceleration from four near-field stations has been made in root mean square sense to finalize several rupture parameters such as dip, strike, rake and starting point of rupture. The actual and simulated records have been compared in terms of root mean square error (RMSE) of peak ground acceleration from both components of acceleration records. Waveform and parameter comparison of strong motion records confirm the efficacy of modified semi-empirical technique for modelling of strong ground motion.

Acknowledgments We are grateful for the valuable comments made by the referees of this paper. The work presented in this paper is an outcome of the sponsored project from Department of Science and Technology (DST), Government of India, with project reference No. GITA/DST/TWN/P-52/2013. Authors sincerely thank Indian Institute of Technology Roorkee and MHRD for supporting the research work presented in this paper. The acceleration waveform data have been obtained from the database (Geophysical Database Management System, GDMS) of Central Weather Bureau (CWB). TheVs30 values at the four stations used for the SHAKE91 calculation are from the Engineering Geological Database for TSMIP (EGDT) (source: http://egdt.ncree.org.tw/), which is thankfully acknowledged.

References

Aki K, Richards PG (2002) Quantitative seismology. University Science Books, Sausalito

Atkinson GM, Boore DM (1995) Ground-motion relation for eastern North America. Bull Seismol Soc Am 85:17–30

Boore DM (1983) Stochastic simulation of high frequency ground motion based on seismological models of radiated Spectra. Bull Seismol Soc Am 73:1865–1894

Boore DM, Atkinson G (1987) Stochastic prediction of ground motion and spectral response parameters at hard-rock sites in eastern North America. Bull Seismol Soc Am 73:1865–1894

Brune JN (1970) Tectonic stress and spectra of seismic shear waves from earthquakes. J Geophys Res 75:4997–5009

Brune JN (1971) Correction. J Geophys Res 76:5002

Central Geological Survey (2000) Taiwan geological map (1:500,000). CGS, MOEA

Hadley DM, Helmberger DV (1980) Simulation of ground motions. Bull Seismol Soc Am 70:617–630

Hanks TC, McGuire RK (1981) The character of high frequency ground motion. Bull Seismol Soc Am 71:2071–2095

Hartzell SH (1978) Earthquake aftershocks as Green's functions. Geophys Res Lett 5:1–4

Hartzell SH (1982) Simulation of ground accelerations for May 1980 Mammoth Lakes, California earthquakes. Bull Seismol Soc Am 72:2381–2387

Housner GW, Jennings PC (1964) Generation of artificial earthquakes. Proc ASCE 90:113–150

Hutchings L (1985) Modeling earthquakes with empirical Green's functions (abs). Earthquake Notes 56:14

Idriss IM, Sun JI (1992) SHAKE91: a computer program for conducting equivalent linear seismic response analyses of horizontally layered soil deposits, Davis, California, Center for Geotechnical Modeling, Department of Civil and Environmental Engineering, University of California

Irikura K (1983) Semi empirical estimation of strong ground motion during large earthquakes. Bull Dis Prevent Res Inst 33:63–104

Irikura K (1986) Prediction of strong acceleration motion using empirical Green's function. In: Proceedings of 7th Japan earthquake engineering symposium, pp 151–156

Irikura K, Kamae K (1994) Estimation of strong ground motion in broad-frequency band based on a seismic source scaling model and an Empirical Green's function technique. Ann Geofis XXXVII 6:1721–1743

Irikura K, Muramatu I (1982) Synthesis of strong ground motions from large earthquakes using observed seismograms of small events. In: Proceedings of the third international microzonation conference, Seattle, pp 447–458

Irikura K, Kagawa T, Sekiguchi H (1997) Revision of the empirical Green's function method by Irikura, 1986. Programme and abstracts. The Seismological Society of Japan 2:B25

Joshi A (2001) Strong motion modelling of the source of the Chamoli earthquake of March 29, 1999 in the Garhwal Himalaya, India. J Seismol 5:499–518

Joshi A (2004) A simplified technique for simulating wide band strong ground motion for two recent Himalaya earthquakes. Pure Appl Geophys 161:1777–1805
Joshi A, Midorikawa S (2004) A simplified method for simulation of strong ground motion using rupture model of the earthquake source. J Seismol 8:467–484
Joshi A, Mohan K (2008) Simulation of accelerograms from simplified deterministic approach for the 23rd October 2004 Niigata-ken Chuetsu earthquake. J Seismol 12:35–51
Joshi A, Patel RC (1997) Modelling of active lineaments for predictions a possible earthquake scenario around Dehradun, Garhwal Himalaya, India. Tectonophysics 283:289–310
Joshi A, Kumar B, Sinvhal A, Sinvhal H (1999) Generation of synthetic accelerograms by modelling of rupture plane. J Earth Tech 36:43–60
Joshi A, Sing S, Giroti K (2001) The simulation of ground motions using envelope summations. Pure Appl Geophys 158:877–901
Joshi A, Kumari P, Sharma ML, Ghosh AK, Agarwal MK, Ravikiran A (2012a) A strong motion model of the 2004 great Sumatra earthquake: simulation using a modified semi empirical method. J Earthq Tsunami 6:1–29
Joshi A, Kumari P, Singh S, Sharma ML (2012b) Near-field and far-field simulation of accelerograms of Sikkim earthquake of September 18, 2011 using modified semi-empirical approach. Nat Hazard 64:1029–1054
Joshi A, Sandeep, Kamal (2014) Modelling of strong motion generation areas of the 2011 Tohoku, Japan earthquake using modified semi empirical technique. Nat Hazard 71:587–609
Kamae K, Kawabe H (2004) Source model composed of asperities for the 2003 Tokachi-oki, Japan, earthquake ($MJMA = 8.0$) estimated by the empirical Green's function method. Earth Planets Space 56:323–327
Kameda H, Sugito M (1978) Prediction of strong earthquake motions by evolutionary process model. In: Proceedings of the sixth Japan earthquake engineering symposium, pp 41–48
Kanai K (1951) relation between the nature of surface layer and amplitude of earthquake motions Bulletin, Tokyo Earthquake Research Institute
Kanamori H (1979) A semi empirical approach to prediction of long period ground motions from great earthquakes. Bull Seismol Soc Am 69:1645–1670
Kanamori H, Anderson DL (1975) Theoretical basis of some empirical relations in seismology. Bull Seismol Soc Am 65:1073–1095
Kumar D, Khattri KN (1999) Average Intrinsic Qs in the crust and upper most 8 km of Mantle in the Ganga Plains, Bihar. Curr Sci 77:748–749
Kuo CH, Wen KL, Hsieh HH, Lin CM, Chang TM, Kuo KW (2012) Site classification and Vs30 estimation of free-field TSMIP stations using the logging data of EGDT. Eng Geol 129–130:68–75
Lai SP (1982) Statistical characterization of strong ground motions using power spectral density function. Bull Seismol Soc Am 72:259–274
Lay T, Wallace TC (1995) Modern Global Seismology (Academic Press, California, 521 pp)
Lee SJ (2013) Real-time moment tensor and ground motion simulation. 0327 Nantou Earthquake Workshop, IES, Taipei, Taiwan
Lin CW, Lu ST, Shin TS, Lin WH, Liu YC, Chen PT (2008) Active faults of central Taiwan: explanatory text of the strip maps of active faults scale 1:25,000. Central Geological Survey Special Publication No. 21, CGS MOEA, Taipei, Taiwan, Republic of China
Lin CM, Chang TM, Wen KL, Kuo CH, Hsieh HH (2014) Seismic structure beneath decollement inferred from 2009/11/5 ML 6.2 Mingjian Earthquake in Central Taiwan. Terr. Atmos. Ocean Sci. 25(1):27–38
Liu KS, Shin TC, Tsai YB (1999) A Free-field strong motion network in Taiwan: TSMIP. Terr. Atmos. Ocean Sci. 10(2):377–396
Lysmer J, Seed HB, Schnable PB (1971) Influence of base rock characteristics on ground response. Bull Seismol Soc Am. 61:1213–1232
Matthiesen RB, Duke CM, Leeds DJ, Fraser JC (1964) Site characteristic of southern California strong motion earthquake stations, part two report No. 64-15, Department of Engineering, University of California, Los Angeles, August
Mei-I Ho (1994) Three-dimensional velocity structure in western Taiwan. Master Thesis, Geophysical Institute, National Central University
Mendoza C, Hartzell S (1988) Inversion for slip distribution using teleseismic P waveforms, North Palm Springs, Borah Peak, and Michoacan earthquakes. Bull Seismol Soc Am 78:1092–1111
Meng CY (1971) A conception of the evolution of the island of Taiwan and its bearing on the development of the western Neogene sedimentary basins. Petrol. Geol. Taiwan 9:241–258
Midorikawa S (1993) Semi empirical estimation of peak ground acceleration from large earthquakes. Tectonophysics 218:287–295

Mikumo T, Irikura K, Imagawa K (1981) Near field strong motion synthesis from foreshock and aftershock records and rupture process of the main shock fault (abs.). IASPEI 21st General Assembly, London

Miyahara M, Sasatani T (2004) Estimation of source process of the 1994 Sanriku Haruka-oki earthquake using empirical Green's function method. Geophys Bull Hokkaido Univ Sapporo Japan 67:197–212 (in Japanese with English abstract)

Miyake H, Iwata T, Irikura K (2003) Source characterization for broadband ground-motion simulation: kinematic heterogeneous source model and strong motion generation area. Bull Seismol Soc Am 93:2531–2545

Munguia L, Brune JM (1984) Simulations of strong ground motions for earthquakes in the Mexicali-Imperial Valley. In: Proceedings of workshop on strong ground motion simulation and earthquake engineering applications, Pub. 85-02. Earthquake Engineering Research Institute, Los Altos, California 21-1-21-19

Papageorgiou A, Aki K (1983) A specific barrier model for the quantitative description of inhomogeneous faulting and the prediction of strong ground motion. Part 1. Description of the model. Bull Seismol Soc Am 73:693–722

Roesset JM, Whitman RV (1969) Theoretical background for amplification studies, Research Report No. R69-15. Soils Publications No. 231, Massachusetts Institute of Technology, Cambridge

Saikia CK (1993) Ground motion studies in great los angels due to $M_w = 7.0$ earthquake on the Elysian thrust fault. Bull Seismol Soc Am 83:780–810

Saikia CK, Herrmann RB (1985) Application of waveform modelling to determine focal mechanism of Four 1982 Miramichi Aftershocks. Bull Seismol Soc Am 75:1021–1040

Schnabel PB, Lysmer J, Seed HB (1972) SHAKE: a computer program for earthquake response analysis of horizontally layered sites Report No. UCB/EERC-72/12, Earthquake Engineering Research Center, University of California, Berkeley

Seno T (1977) The instantaneous rotation vector of the Philippine sea plate relative to the Eurasia plate. Tectonophysics 42:209–226

Shin TC, Chang CH, Pu HC, Lin HW, Leu PL (2013) The geophysical database management system in Taiwan. Terr Atmos Ocean Sci 24(1):11–18

Sokolov V, Wen KL, Miksat J, Wenzel F, Chen CT (2009) Analysis of Taipei basin response for earthquakes of various depths and locations using empirical data. Terr Atmos Ocean Sci 20:687–702

Suzuki W, Iwata T (2007) Source model of the 2005 Miyagi-Oki, Japan, earthquake estimated from broadband strong motions. Earth Planets Space 59:1155–1171

Takiguchi M, Asano K, Iwata T (2011) The comparison of source models of repeating subduction-zone earthquakes estimated using broadband strong motion records–1982 and 2008 Ibaraki-ken-oki M7 earthquakes. J Seism Soc Jpn 63:223–242 (in Japanese with English abstract)

Wessel P, Smith WHF (1991) Free software helps map and display data. EOS Trans AGU 72(441):445–446

Yu G (1994) Some aspects of earthquake seismology: slip portioning along major convergent plate boundaries: composite source model for estimation of strong motion and non linear soil response modeling. Ph.D. thesis, University of Nevada

Yu G, Khattri KN, Anderson JG, Brune JN, Zeng Y (1995) Strong ground motion from the Uttarkashi, Himalaya, India, earthquake: comparison of observations with synthetics using the composite source model. Bull Seismol Soc Am 85:31–50

Yu SB, Chen HY, Kuo LC (1997) Velocity field of GPS stations in the Taiwan area. Tectonophysics 274:41–59

Zeng Y, Anderson JG, Su F (1994) A composite source model for computing realistic synthetic strong ground motions. Geophys Res Lett 21:725–728